Tuning Dzyaloshinskii-Moriya interactions in magnetic bilayers with a ferroelectric substrate

B. H. Zhang,[1] Y. S. Hou,[2] Z. Wang,[1] and R. Q. Wu[2,*]

[1]*State Key Laboratory of Surface Physics, Key Laboratory of Computational Physical Sciences, and Department of Physics, Fudan University, Shanghai 200433, China*

[2]*Department of Physics and Astronomy, University of California, Irvine, California 92697, USA*

(Received 17 September 2020; revised 21 December 2020; accepted 25 January 2021; published 10 February 2021)

We performed systematic first-principles calculations to explore the possibility of manipulating Dzyaloshinskii-Moriya interactions (DMIs) in heavy metal/ferromagnetic metal bilayers with ferroelectric (FE) polarization of a $PbTiO_3$ (PTO) substrate. Significantly, both the sign and magnitude of the DMI can be tailored by the FE polarization reversal in PTO. Moreover, the DMIs of Ir/Co/PTO and Ir/Fe/PTO can achieve large values ($|d| > 10$ meV) under the influence of an upward electric polarization of PTO. Our findings provided useful strategies for enhancing and tailoring DMIs in complex heterostructures and paved the way for the development of DMI-based devices with ultralow power consumption.

DOI: 10.1103/PhysRevB.103.054417

I. INTRODUCTION

There is currently a significant exploration of solid-state materials that can enable coherent manipulation of magnetic properties by an electric field, instead of a magnetic field or electric current, as a pathway toward a new level of performance and energy efficiency within the realms of quantum computing and spintronics. One of the frontiers is to enhance and control Dzyaloshinskii-Moriya interaction (DMI) [1,2] in magnetic materials as DMI plays an essential role in many exotic phenomena such as multiferroicity [3], magnon Hall effect [4–7], exchange bias [8], magnetic skyrmions [9–11], and chiral domain walls (DWs) [12,13]. Experimental measurements using Brillouin light scattering spectroscopy [14,15], Lorentz transmission electron microscopy [16], and scanning electron microscopy [17], as well as theoretical studies (e.g., with the spin-wave theory [18,19] and Berry phase theory [20]) have provided clear evidence for the presence of DMI in several bulk materials [21,22] and interfaces [23,24]. In particular, the heavy metal (HM)/ferromagnetic metal (FM) heterostructures have been identified as potential combinations for the production of large interfacial DMI. [25] Nevertheless, DMIs in most existing cases are still too small, and it is hence of practical importance to find viable strategies for enhancing and tuning DMIs in a large range for the technological developments.

Many different approaches, such as proximity [26], doping [27], current [28], and voltage and electric field [29,30], have been attempted for achieving the enhancement and control of DMI. Studies of DMIs in heterostructures with ultrathin HM/FM films on ferroelectric (FE) substrates have just started getting attention [31,32]. With their nonvolatile and switchable electric polarization, FE substrates may maximize the symmetry reduction at interfaces and provide efficient local control of magnetic properties. This is exciting as the energy cost for electric polarization reversal is also much smaller than that of other means for the control of magnetic properties. Therefore, it is especially important to perform systematic investigations of the interplay of magnetization, spin-orbit coupling (SOC), and strong local electric polarization and field to produce large DMIs in these complex heterostructures.

In this work, we used first-principles calculations to systematically investigate the DMI for HM/FM/$PbTiO_3$ (HM = Ir, Pt, Au, and FM = Fe, Co). We found that the sign and magnitude of the DMI can be manipulated by reversing electric polarization directions of the ferroelectric $PbTiO_3$ (PTO). In particular, the DMIs of Ir/Co/PTO and Ir/Fe/PTO with an upward polarization (P_{up}) can achieve exceptionally large values ($|d| > 10$ meV), and the DMI of Pt/Co/PTO may even change sign by reversing the electric polarization of PTO. The dramatic enhancement or sign change of DMI mainly results from the interplay among the HM's strong SOC, FM's magnetization, and PTO's local electric field. Our work demonstrates the possibility of making reversible and nonvolatile control of DMIs in a large range, and provides a promising strategy for designing functional materials for spintronic applications.

II. METHODS

The first-principles calculations were performed using the projector augmented wave (PAW) method as implemented in the Vienna *ab initio* simulation package (VASP). The exchange-correlation interactions were described by the generalized-gradient approximation (GGA) with the Perdew-Burke-Ernzerhof (PBE) functional [33]. An energy cutoff of 550 eV was used for the plane-wave basis expansion. To simulate the epitaxially grown HM/FM/PTO heterostructure, we constructed a slab model as shown in Figs. 1(a) and 1(b), in which we stacked one HM layer and one FM layer on $1 \times 1 \times 3$ cubic cells of PTO, with the TiO_2 terminated surface in contact with the FM layers [34]. At the interface, atoms

*wur@uci.edu

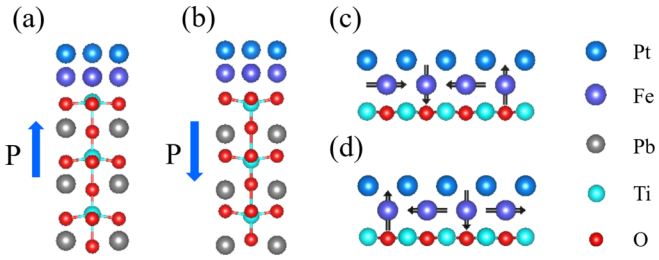

FIG. 1. Atomic structures of HM/FM/PTO heterostructures with the electric polarization of PTO layer aligning along (a) up (P_{up}) and (b) down (P_{dn}) directions. Examples of (c) clockwise and (d) counterclockwise spin configurations used for the determination of the DMI.

of the FM layer sit above the topmost O atoms of the PTO substrate (see Part I in the Supplemental Material for comparison of different stacking modes [35]). In order to avoid artificial interaction between periodic images, a vacuum space of 12 Å was inserted between periodic slabs of atoms. The in-plane lattice constant was fixed at the experimental value of the bulk PTO ($a = b = 3.90$ Å). During the structural optimization procedures atom positions of the bottom two PTO cubic cells were fixed to their bulk values of upward and downward electric polarizations while positions of all other atoms were fully relaxed using the conjugate gradient method until the force acting on each atom became less than 0.01 eV/Å. The Brillouin zone was sampled with a $12 \times 12 \times 1$ k-point mesh for the primitive cell and a denser $24 \times 24 \times 1$ k-point mesh was used to calculate the magnetic anisotropy energy (MAE). The DMIs were obtained by using the chirality-dependent total energy difference approach [36], in which a $2\sqrt{2} \times \sqrt{2} \times 1$ supercell and a $9 \times 18 \times 1$ k mesh were adopted.

III. RESULTS AND DISCUSSIONS

At the FE phase, PTO exhibits a FE polarization pointing along the (001) direction. For the convenience of discussions, we denote the electric polarization as P_{up} when it points toward HM/FM and P_{dn} for the opposite. The FE reversal produces notable changes in the charge transfer between PTO and metal layers. To demonstrate this, we take Ir/Co/PTO as an example, and plot the charge redistribution in Fig. 2. Obviously, more charge transfer between O and Co atoms occurs in the P_{dn} state, whereas charge rearrangement mainly happens between Co and Ti atoms in the P_{up} state. It is much clearer to see this from the Bader charge analyses in Table I. Note that the Co atom loses 0.037 e and the Ti atom gains 0.069 e in comparison to the atoms in the freestanding PTO and Ir/Co layers in the P_{up} state. In the P_{dn} state, the Co atom loses 0.211e and the O atom gains 0.172 e in contrast to the freestanding systems. The interface atoms tend to have more charge in the P_{up} state than in the P_{dn} state. In addition, significant differences can be seen from the layer-resolved projected density of states (PDOS) in Fig. 2, the PDOS of different PTO layers shift oppositely in the P_{up} and P_{dn} states, due to the internal electric field within PTO established by the electric polarization [37]. As a result, the conduction band minimum (valence band maximum) of PTO touches the Fermi level in the P_{up} (P_{dn}) state. The interfacial hybridizations are also altered as we reverse the electric polarization, which is expected to affect the electronic and magnetic properties of FM atoms very differently, as seen from the PDOS curves of Co in the minority spin channel. Considering that the FE properties can be affected by electrodes [38], we give the results of Ir/Co/PTO with Pd electrodes for comparison (more results are shown in Part II in the Supplemental Material [35]). It appears that the presence of electrodes has very little effect on the magnetic properties and DMI. Therefore, in the following study we only focus on the HM/FM/PTO heterostructures without electrodes, unless stated otherwise.

Now we study the magnetic properties of a series of HM/FM/PTO heterostructures. As shown in Fig. S2(a) [35], for the freestanding HM/FM bilayers, the magnetic moments of FM layers do not change much (~2 μ_B for Co and ~3 μ_B for Fe) when they are in contact with different HM overlayers. After introducing the PTO substrate, the magnetic moments of FM atoms in the P_{up} state become smaller than those in the P_{dn}

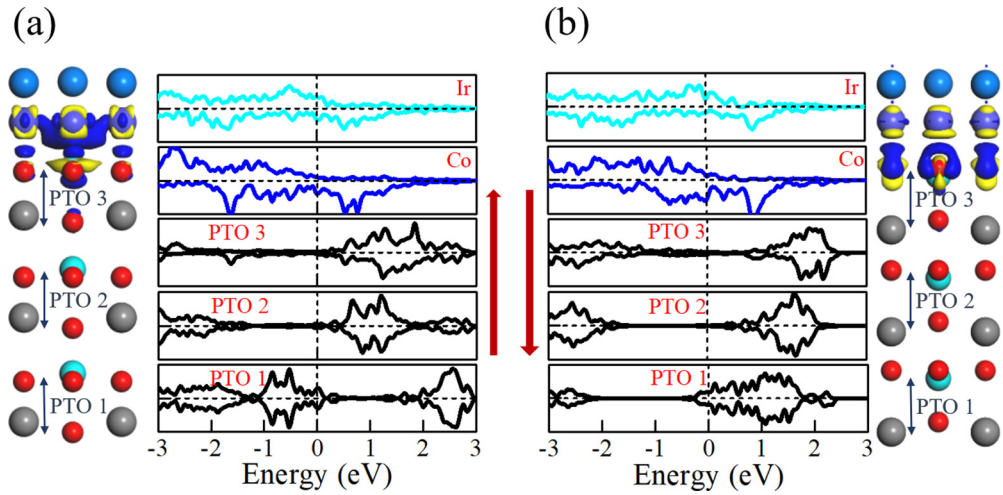

FIG. 2. Charge density difference and PDOS of Ir/Co/PTO for (a) P_{up} and (b) P_{dn} polarization. Blue and yellow regions show charge accumulation and depletion, respectively.

TABLE I. Bader charges of atoms at the interface. The charge differences between Ir/Co/PTO heterostructures and freestanding PTO and Ir/Co are listed in parentheses. The positive sign means gaining more electrons and the negative sign means the opposite. The last row gives the differences between values in the first two rows (P_{up} and P_{dn}).

Element	O	Ti	Co	Ir
P_{up}	7.400 (−0.014)	1.694 (+0.069)	8.595 (−0.037)	9.362 (−0.006)
P_{dn}	7.284 (+0.172)	1.483 (+0.045)	8.412 (−0.211)	9.381 (+0.004)
Difference between P_{up} and P_{dn}	+0.116	+0.211	+0.183	−0.019

state. In Fig. S2(b) [35], we also give the magnetic moments of the HM layers. Clearly, the Ir and Pt atoms acquire large induced magnetic moments, while Au remains magnetically dead.

In Fig. S2(c) [35], we show the MAEs of these HM/FM/PTO heterostructures. It is interesting to note that the MAEs of Ir/Co and Pt/Co are significantly changed by the PTO substrate, especially in the P_{dn} state. For Pt/Co/PTO, the MAE can be turned from negative (prefers an in-plane magnetization) to positive (prefers an out-of-plane magnetization) when the electric polarization in PTO changes its direction. For Ir/Co/PTO, the MAEs are greatly enhanced in both P_{up} and P_{dn} states, compared with that of the unsupported Ir/Co. In order to appreciate the mechanism of the altered MAE in these systems, we plot the MAE as a function of the position of the Fermi level (E_F) according to the rigid band model and torque method [39,40]. As shown in Fig. 3, the total MAE of Ir/Co rapidly increases when the E_F shifts downward and may reach to about 17 meV when E_F is lowered by −0.15 eV from its natural position E_F^0. On the other hand, MAE may change its sign if we shift E_F upward by +0.21 eV. Roughly, the electric polarization causes the MAE(E_F) curve to shift to the left (P_{up}) or right (P_{dn}) side, showing the effect of charge transfer. Similar behavior is also found for the MAE(E_F) dependence of Pt/Co, although the trend for the P_{up} state appears to be more complicated. The MAE of Pt/Co/PTO in the P_{dn} state has a shoulder at E_F^0 and can be easily more positive if E_F lowers, possibly by applying an external electric field or strain. Since both MAE and DMI stem from the interplay between magnetization and SOC, we perceive that the DMI of Ir/Co and Pt/Co may also change dramatically with the reversal of the FE polarization of PTO. We also calculate the MAE of Ir/Co/PTO with different layers of PTO and found that three cubic cells of PTO are adequate (see Table S2 in Part VII in the Supplemental Material [35]).

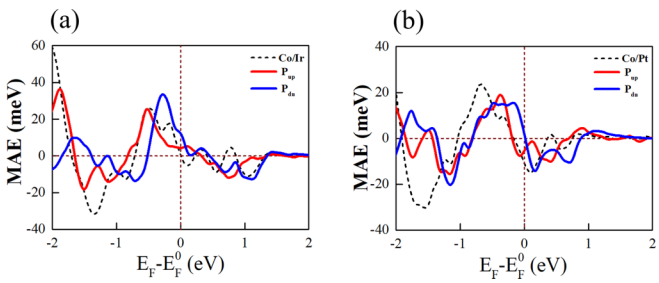

FIG. 3. Fermi level dependent total MAEs from the rigid band model of (a)Ir/Co and Ir/Co/PTO systems and (b) Pt/Co and Pt/Co/PTO systems.

To validate this plausible conjecture, we determine the antisymmetric spin exchange interactions as [36,41,42]

$$E_{\mathrm{DMI}} = \mathbf{d}_{ij} \cdot (\mathbf{S}_i \times \mathbf{S}_j), \tag{1}$$

where $\mathbf{S}_i$ and $\mathbf{S}_j$ are spin moments sitting on neighboring atomic sites i and j, and $\mathbf{d}_{ij}$ (the scalar value is denoted by d) is a characteristic DMI vector. The microscopic DMI strength can be derived according to the chirality-dependent total energy difference approach [36]:

$$d = (E_{\mathrm{CW}} - E_{\mathrm{ACW}})/m, \tag{2}$$

with the chiral magnetic configurations shown in Figs. 1(c) and 1(d). E_{CW} and E_{ACW} represent the energy of clockwise and counterclockwise spin configurations, respectively. Note that the magnetic moments of these two configurations are almost the same from DFT calculations, which ensures the validity of the present approach. The number m is 16 in our calculations (details are given in Part IV in the Supplemental Material [35]). The micromagnetic DMI strength of the bilayer can be inferred by the micromagnetic energy per volume unit of the magnetic film [36]:

$$E = D\left[m_z \frac{dm_x}{dx} - m_x \frac{dm_z}{dx}\right], \tag{3}$$

where $D = \frac{4d}{N_F a^2}$ with a the lattice constant and N_F the number of magnetic layers ($N_F = 1$ here; see Part V in the Supplemental Material [35]). The positive and negative signs of d and D indicate the anticlockwise (left) and clockwise (right) chirality, respectively.

As seen in Fig. 4(a) for freestanding HM/FM structure, the largest DMI can reach up to $d = 13.86$ meV in the Pt/Fe bilayer, while Au/Co and Ir/Fe also exhibit considerable DMIs but with an opposite sign (see Fig. S4 for D [35]). We want to point out that the calculated parameter d is almost independent of the choice of the spin spirals. To show this, we take the Pt/Fe bilayer as an example. When we set the spin spiral with 60° and 45°, the change of d is within 8% from the 90° spin spiral. By putting HM/FM on PTO and switching the FE polarization, the DMI strengths of Ir/Fe and Pt/Fe remain large but the response to the reversal of electric polarization is not as high as desired. Strikingly, the sign and magnitude of DMI of Ir/Co and Pt/Co can be strongly modulated. The P_{up} polarization in PTO can enhance the DMI of Ir/Co/PTO by ∼8.8 times and change its sign compared to that of the unsupported Ir/Co bilayer. If we change the polarization of PTO to zero, i.e., by placing all ions at the local centrosymmetric positions (see Table S3 in the Supplemental Material [35]), the DMI is about halved. This clearly indicates that the local electric field produced by the polarization rather than the interfacial

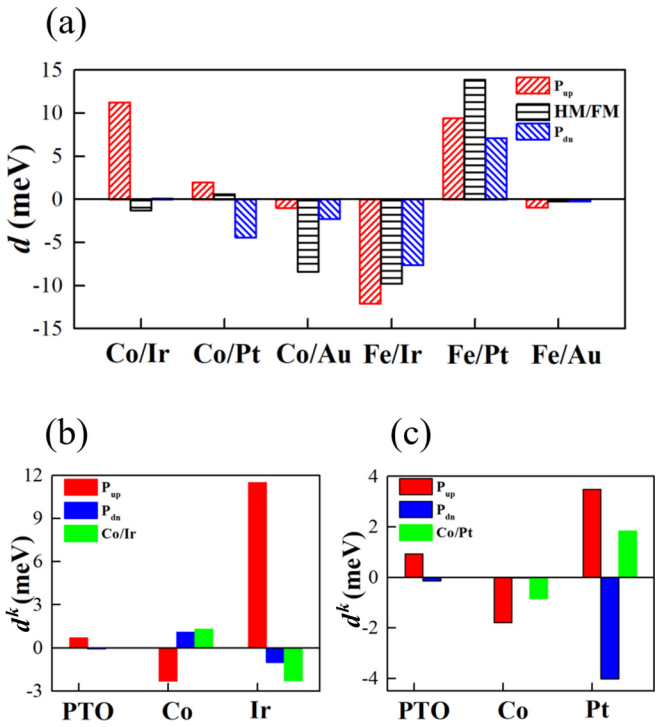

FIG. 4. (a) The DMI coefficients d of the HM/FM bilayers and HM/FM/PTO systems with P_{up} and P_{dn} polarizations. The calculated layer-resolved DMI coefficient d^k of (b) the Ir/Co bilayer and Ir/Co/PTO heterostructure and (c) the Pt/Co bilayer and Pt/Co/PTO heterostructure.

hybridization plays the most important role in determining DMI. In contrast, the MAE remains close to that in the P_{up} state as it is a local effect and mostly depends on the arrangements of d orbitals of transition metal atoms. Note that the physical properties somewhat depend on the thickness of the HM, especially in the monolayer regime. We test Ir/Co/PTO with bilayer Ir and find that both MAE and DMI may change by the addition of the It layer. This is understandable since the bands of the interfacial Ir layer are much broadened as the Ir-Co hybridization is also altered. As the monolayer is the most interesting and sensitive case for metallic layers with the least screening effect, we hope our models can be realized in experiments using the ultrahigh vacuum molecular epitaxy growth. Nevertheless, reversing the electric polarization still plays an important role in altering DMIs of 2Ir/Co/PTO (see Tables S4 and S5 in the Supplemental Material [35]).

Pt/Co/PTO can also change DMI from positive to negative with P_{dn} polarization, even though the magnitude of DMI is relatively smaller. In order to elucidate the remarkable changes of DMI driven by the FE polarization in Ir/Co/PTO and Pt/Co/PTO, we calculate the DMI by selectively switching on the SOC of different layers, d^k [36,41]. The results are shown in Figs. 4(b) and 4(c); it is worth noting that the sign and strength of DMI are mainly contributed by the SOC of the HM layers, which agree well with previous studies [41]. In all cases, the SOC of the FM layers contributes opposite DMIs, a status which is rather counterintuitive. The contributions from the PTO's SOC are generally small but not negligible in the P_{up} state. To sum up, switching the FE polarization changes the DMI contributions from HM layers, mainly via local electric field and the interplay with the strong SOC in the HM layer. This is somewhat like the generation of the Rashba effect and hence it is not a surprise that these to effects can be interconnected. As shown in Part VIII in the Supplemental Material [35], the Rashba effect on the band structure is obvious and the Rashba coefficient also changes sign as the polarization of PTO is reversed. However, the Rashba coefficient varies from band to band and hence the quantitative connection to DMI is unobvious.

IV. CONCLUSIONS

In conclusion, we systematically investigated the possibility of tuning electronic and magnetic properties of HM/FM bilayers with FE polarization of the PTO substrate by means of first-principles calculations. Significantly, both their MAEs and DMIs can be altered in a large range or, for some cases, even in sign by reversing the electric polarization, which paves the way to tailoring these crucial magnetic properties without the need of large current or magnetic field. In particular, our calculations indicated that the DMI of Ir/Co/PTO and Ir/Fe/PTO can reach exceedingly high values ($|d| > 10$ meV) with the polarization P_{up} of PTO layers, and the sign of DMI of Pt/Co/PTO can flip with the switch between P_{up} and P_{dn}. The large change of DMI results from the interplay among the SOC in HM, magnetization in FM, and the local electric field from PTO. Our results and insights suggest an alternative strategy for the design of DMI-based spintronic materials and open a vista for the design of energy efficient devices. For example, as the chirality and size of magnetic skyrmions are tightly connected to DMI [43], this means that one can manipulate the skyrmion density and chirality using FE substrates—a very convenient strategy.

ACKNOWLEDGMENTS

The work was supported by the U.S. DOE-Basic Energy Science under Grant No. DE-FG02-05ER46237 and computational time at National Energy Research Scientific Computing Center.

[1] I. Dzyaloshinsky, J. Phys. Chnem. Solids **4**, 241 (1958).
[2] T. Moriya, Phys. Rev. Lett. **4**, 228 (1960).
[3] K. F. Wang, J. M. Liu, and Z. F. Ren, Adv. Phys. **58**, 321 (2009).
[4] Y. Onose, T. Ideue, H. Katsura, Y. Shiomi, N. Nagaosa, and Y. Tokura, Science **329**, 297 (2010).
[5] J. Jiang, D. Xiao, F. Wang, J.-H. Shin, D. Andreoli, J. Zhang, R. Xiao, Y.-F. Zhao, M. Kayyalha, L. Zhang, K. Wang, J. Zang, C. Liu, N. Samarth, M. H. W. Chan, and C.-Z. Chang, Nat. Mater. **19**, 732 (2020).
[6] J. Matsuno, N. Ogawa, K. Yasuda, F. Kagawa, W. Koshibae, N. Nagaosa, Y. Tokura, and M. Kawasaki, Sci. Adv. **2**, e1600304 (2016).
[7] K. Y. Meng, A. S. Ahmed, M. Bacani, A. O. Mandru, X. Zhao, N. Bagues, B. D. Esser, J. Flores, D. W.

McComb, H. J. Hug, and F. Y. Yang, Nano Lett. **19**, 3169 (2019).
[8] S. Dong, K. Yamauchi, S. Yunoki, R. Yu, S. Liang, A. Moreo, J. M. Liu, S. Picozzi, and E. Dagotto, Phys. Rev. Lett. **103**, 127201 (2009).
[9] J. Sampaio, V. Cros, S. Rohart, A. Thiaville, and A. Fert, Nat. Nanotechnol. **8**, 839 (2013).
[10] A. Fert, V. Cros, and J. Sampaio, Nat. Nanotechnol. **8**, 152 (2013).
[11] N. Romming, C. Hanneken, M. Menzel, J. E. Bickel, B. Wolter, K. von Bergmann, A. Kubetzka, and R. Wiesendanger, Science **341**, 636 (2013).
[12] W. W. Wang, M. Albert, M. Beg, M. A. Bisotti, D. Chernyshenko, D. Cortes-Ortuno, I. Hawke, and H. Fangohr, Phys. Rev. Lett. **114**, 087203 (2015).
[13] S. Emori, U. Bauer, S. M. Ahn, E. Martinez, and G. S. D. Beach, Nat. Mater. **12**, 611 (2013).
[14] K. Di, V. L. Zhang, H. S. Lim, S. C. Ng, M. H. Kuok, J. W. Yu, J. B. Yoon, X. P. Qiu, and H. S. Yang, Phys. Rev. Lett. **114**, 047201 (2015).
[15] M. Belmeguenai, J.-P. Adam, Y. Roussigne, S. Eimer, T. Devolder, J.-V. Kim, S. M. Cherif, A. Stashkevich, and A. Thiaville, Phys. Rev. B **91**, 180405(R) (2015).
[16] X. Z. Yu, Y. Onose, N. Kanazawa, J. H. Park, J. H. Han, Y. Matsui, N. Nagaosa, and Y. Tokura, Nature **465**, 901 (2010).
[17] F. Kloodt-Twesten, S. Kuhrau, H. P. Oepen, and R. Fromter, Phys. Rev. B **100**, 100402(R) (2019).
[18] J.-H. Moon, S.-M. Seo, K.-J. Lee, K.-W. Kim, J. Ryu, H.-W. Lee, R. D. McMichael, and M. D. Stiles, Phys. Rev. B **88**, 184404 (2013).
[19] P. Ferriani, K. von Bergmann, E. Y. Vedmedenko, S. Heinze, M. Bode, M. Heide, G. Bihlmayer, S. Blügel, and R. Wiesendanger, Phys. Rev. Lett. **101**, 027201 (2008).
[20] F. Freimuth, S. Blügel, and Y. Mokrousov, J. Phys.: Condens. Matter **26**, 104202 (2014).
[21] S. Muehlbauer, B. Binz, F. Jonietz, C. Pfleiderer, A. Rosch, A. Neubauer, R. Georgii, and P. Boeni, Science **323**, 915 (2009).
[22] C. Pfleiderer, T. Adams, A. Bauer, W. Biberacher, B. Binz, F. Birkelbach, P. Boeni, C. Franz, R. Georgii, M. Janoschek, F. Jonietz, T. Keller, R. Ritz, S. Muehlbauer, W. Muenzer, A. Neubauer, B. Pedersen, and A. Rosch, J. Phys.: Condens. Matter **22**, 164207 (2010).
[23] C. Moreau-Luchaire, C. Moutafis, N. Reyren, J. Sampaio, C. A. F. Vaz, N. Van Horne, K. Bouzehouane, K. Garcia, C. Deranlot, P. Warnicke, P. Wohlhuter, J. M. George, M. Weigand, J. Raabe, V. Cros, and A. Fert, Nat. Nanotechnol. **11**, 444 (2016).
[24] O. Boulle, J. Vogel, H. Yang, S. Pizzini, D. de Souza Chaves, A. Locatelli, T. O. Mentes, A. Sala, L. D. Buda-Prejbeanu, O. Klein, M. Belmeguenai, Y. Roussigne, A. Stashkevich, S. M. Cherif, L. Aballe, M. Foerster, M. Chshiev, S. Auffret, I. M. Miron, and G. Gaudin, Nat. Nanotechnol. **11**, 449 (2016).
[25] A. Fert and P. M. Levy, Phys. Rev. Lett. **44**, 1538 (1980).
[26] D. d. S. Chaves, F. Ajejas, V. Křižáková, J. Vogel, and S. Pizzini, Phys. Rev. B **99**, 144404 (2019).
[27] T. Kikuchi, T. Koretsune, R. Arita, and G. Tatara, Phys. Rev. Lett. **116**, 247201 (2016).
[28] N. Kato, M. Kawaguchi, Y. C. Lau, T. Kikuchi, Y. Nakatani, and M. Hayashi, Phys. Rev. Lett. **122**, 257205 (2019).
[29] T. Srivastava, M. Schott, R. Juge, V. Krizakova, M. Belmeguenai, Y. Roussigne, A. Bernand-Mantel, L. Ranno, S. Pizzini, S. M. Cherif, A. Stashkevich, S. Auffret, O. Boulle, G. Gaudin, M. Chshiev, C. Baraduc, and H. Bea, Nano Lett. **18**, 4871 (2018).
[30] T. Koyama, Y. Nakatani, J. Ieda, and D. Chiba, Sci. Adv. **4**, eaav0265 (2018).
[31] L. F. Wang, Q. Y. Feng, Y. Kim, R. Kim, K. H. Lee, S. D. Pollard, Y. J. Shin, H. B. Zhou, W. Peng, D. Lee, W. J. Meng, H. Yang, J. H. Han, M. Kim, Q. Y. Lu, and T. W. Noh, Nat. Mater. **17**, 1087 (2018).
[32] H. Wang, Y. Dai, Z. Liu, Q. Xie, C. Liu, W. Lin, L. Liu, P. Yang, J. Wang, T. V. Venkatesan, G. M. Chow, H. Tian, Z. Zhang, and J. Chen, Adv. Mater. **32**, 1904415 (2020).
[33] J. P. Perdew, K. Burke, and M. Ernzerhof, Phys. Rev. Lett. **77**, 3865 (1996); **78**, 1396(E) (1997).
[34] C.-G. Duan, S. S. Jaswal, and E. Y. Tsymbal, Phys. Rev. Lett. **97**, 047201 (2006).
[35] See Supplemental Material at http://link.aps.org/supplemental/10.1103/PhysRevB.103.054417 for comparison of different stacking modes; Ir/Co/PTO with Pd electrodes; magnetic moments and MAEs of HM/FM and HM/FM/PTO; details of the derivation of $m = 16$; the micromagnetic DMI constant D; comparison of MAEs and DMIs in different systems; and analysis of DMI from the perspective of Rashba effect.
[36] H. Yang, A. Thiaville, S. Rohart, A. Fert, and M. Chshiev, Phys. Rev. Lett. **115**, 267210 (2015).
[37] A. E. Bocirnea, D. G. Popescu, C. Chirila, R. M. Costescu, V. Kuncser, V. Stancu, L. Trupina, I. Pasuk, A. M. Vlaicu, and M. A. Husanu, Phys. Rev. Mater. **4**, 034402 (2020).
[38] Y. Umeno, B. Meyer, C. Elsässer, and P. Gumbsch, Phys. Rev. B **74**, 060101(R) (2006).
[39] X. D. Wang, R. Q. Wu, D. S. Wang, and A. J. Freeman, Phys. Rev. B **54**, 61 (1996).
[40] J. Hu and R. Wu, Phys. Rev. Lett. **110**, 097202 (2013).
[41] A. Belabbes, G. Bihlmayer, F. Bechstedt, S. Blügel, and A. Manchon, Phys. Rev. Lett. **117**, 247202 (2016).
[42] W. N. Lin, B. S. Yang, A. P. Chen, X. H. Wu, R. Guo, S. H. Chen, L. Liu, Q. D. Xie, X. Y. Shu, Y. J. Hui, G. M. Chow, Y. P. Feng, G. Carlotti, S. Tacchi, H. X. Yang, and J. S. Chen, Phys. Rev. Lett. **124**, 217202 (2020).
[43] Y. Zhu, J. Y. Fan, and R. Q. Wu, J. Magn. Magn. Mater. **507**, 166805 (2020).